Hejian Liu ✉
Zhen Zhang

https://doi.org/10.21278/TOF.501069724
ISSN 1333-1124
eISSN 1849-1391

OPTIMISATION METHOD FOR PARAMETERS OF ENERGY-EFFICIENT AND HIGH-PERFORMANCE PLASMA SPRAY PROCESS

Summary

Plasma spray welding is widely used in surface engineering and remanufacturing. To improve the efficiency of energy utilisation during the spray welding process and the performance of repaired parts, plasma spray welding parameters are optimised from three aspects, namely the efficiency of energy utilisation, the Vickers hardness of the repaired layer, and the residual stress on the boundary of the heat-affected zone on the workpiece surface. Based on the central composite design method, experiments were conducted to analyse the relationship between specific energy, Vickers hardness, residual stress, and process parameters. The objective functions of the energy efficiency, the Vickers hardness, and the residual stress during plasma spray welding were established by using the response surface methodology. A multi-objective optimisation model has been established based on the improved energy efficiency and process performance. Finally, the relationship between the energy efficiency and the repair process performance was discussed.

Key words: *plasma spray welding; energy efficiency; process performance; multi-objective optimisation*

1. Introduction

With the rapid development of surface engineering and remanufacturing, the application of plasma spray welding is increasingly wider. However, the spray welding process requires a large amount of energy and resources; at the same time, waste gas, waste residue, light radiation, etc., adversely affect the environment.

Energy conservation is an effective means of reducing the imbalance between energy supply and demand while being necessary for the protection of the natural environment and ecological resources [1, 2]. The increased use of energy has led to serious environmental concerns, including resource issues and global warming. The industrial sector is responsible for one third of the total energy consumption in the United States [3]. Growing industrial activity continues to increase energy use in the manufacturing industry, which rose by nearly 2% in 2017 [4]. Statistical data for China show that the industry sector is extremely energy intensive and accounts for about 70% of the total energy use. Among the total energy consumption of the industry sector, the machining industry accounts for almost a quarter of the total. However, although the machining industry consumes a large amount of energy, its energy efficiency is quite low.

In recent years, a lot of research has been done on the modelling of energy consumption in order to reduce this consumption during the manufacturing process, leading to a series of interesting results. Wang et al. [5] proposed energy consumption model for a plasma spraying system considering various working states and processing parameters, and verified that the model can accurately calculate energy consumption with an error of less than 5%. Zang et al. [6] applied computational fluid dynamics to simulate changes in the melting state of in-flight particles. Energy consumption depends not only on spraying power but also on spraying time. Aiming at the characteristics of high energy consumption and low energy efficiency of arc welding, Yan et al. [7] proposed a multi-objective optimisation algorithm based on the fitness sharing genetic algorithm (FSGA). Considering the two independent variables of welding current and welding speed, energy consumption and thermal efficiency were selected as optimisation objectives. Finally, E360 steel was taken as an example to verify the effectiveness of the proposed method with respect to energy saving and thermal efficiency improvement. Liu et al. [8] optimised the laser energy consumption and cost of the welding process using the running time and operating state of the laser arc welding as optimised variables. Tian et al. [9] built a multi-objective optimisation model for the injection moulding process using the Tiankou method and the non-dominated sorting genetic algorithm. The results showed that the model not only improved the stability of the injection moulding process but also reduced the energy consumption during product processing. Sproesser et al. [10] evaluated the efficiency of single-wire gas metal arc welding (SGMAW) and high-power series melting electrode gas protection welding (TGMAW). The results showed that energy efficiency can be increased by 24%, and welding time can be reduced by over 50% using the tandem processes. Pastras et al. [11] analysed the laser welding technology and the welding energy efficiency. Finally, the influence of the energy efficiency and the weld pool geometry on process parameters was studied and discussed. Zhang et al. [12] proposed a novel energy consumption modelling and prediction approach for a milling process from a multistage perspective. Ding et al. [13] developed an integrated modelling methodology to quantify the energy consumption and equivalent carbon footprint in the grinding process.

In the plasma spray welding repair process, different processing parameters not only affect the energy consumption but also have an important impact on the mechanical properties of the repaired workpiece, such as residual stress [14] and the Vickers hardness [15]. In a study on the coating residual stress, Wang et al. [16] prepared a stable zirconia (YSZ) thermal barrier coating by plasma spraying and characterised the residual stress of the coating under different spraying power. The results showed that the increase in spraying power increases the residual stress of the coating and shortens the thermal shock life of the coating. Cheng et al. [17] studied the thermodynamic response behaviour during laser directional deposition, and established a quantitative relationship between temperature gradient, thermal strain, and residual stress by studying the influence of process parameters (laser power and scanning speed) on thermal strain and residual stress. The results showed that the residual stress of a sample can be effectively reduced by optimising the process parameters. In terms of the influence of process parameters on hardness, Raden Dadan et al. [18] conducted a study on the influence of spraying distance on microstructure and hardness, and the results showed that when the thermal spraying distance was 30 cm, the thermal spraying area reached the maximum hardness value. Han et al. [19] selected different spraying distances, spraying power, and powder delivery rates for experimental investigation on the performance of plasma-sprayed coatings and predicted the coating performance based on a backpropagation artificial neural network model. The results showed that the sample coating was best prepared when the spraying distance was 127 mm, the powder delivery speed was 38 g/min, and the spraying power was 34 kW. Tao et al. [20] applied a second-order regression model to establish the empirical relationship between process parameters and tensile strength. The central composite design method was used to obtain the

input-output data. The developed model was tested for its adequacy and significance. Kumar et al. [21] used the Taguchi method and gray correlation analysis to optimise the process parameters of the generic thermal barrier coating.

In conclusion, energy efficiency and process performance optimisation of the welding process have been widely studied, however, separately. Less comprehensive research has been conducted on the energy consumption of the welding process and the process performance of the repaired parts as the optimisation target.

Therefore, this study aimed to obtain optimum spray welding process performance and high energy efficiency, the topics that have been the focus of several multi-objective optimisation studies. Firstly, the energy consumption characteristics and the performance of the plasma spray welding process were analysed. Secondly, central composite design (CCD) was used to analyse the relationship between specific energy, the Vickers hardness, residual stress, and process parameters in the plasma spray welding process. The reliability of the model was verified by the regression equation obtained by the response surface method. Finally, an optimal solution set was obtained using the non-dominated sorting genetic algorithm based on the actual constraints. The relationship between energy efficiency and process performance of the repaired piece was also established.

2. Process optimisation target analysis

Plasma spray welding can make full use of the characteristics of materials sprayed on the surface of metal parts, which makes it possible to obtain excellent performance under various working conditions. This technique can reduce the production cost. However, like other welding processes, plasma spray welding is also energy-consuming. Because of numerous process parameters, the processability of the products varies a lot depending on these parameters. In order to obtain high energy efficiency and high-quality repaired parts, the parameters in the plasma spray welding process have been optimised in this paper. The specific energy was taken as the energy consumption index of the process. In addition, the Vickers hardness and residual stress, which have a great impact on the performance of the repair process, were selected as the criteria.

2.1 Characterisation of the energy utilisation rate of plasma spray welding

Specific energy can be used as an index to measure energy consumption in machining processes [22]. To explore the relationship between a parameter in the welding process and energy consumption, specific energy consumption (SEC) was applied, which refers to the ratio of the total energy consumed by the plasma spray welding and the material weight consumed during the spraying process. The unit of SEC is kJ/g. It can be shown from the definition that the lower the SEC value is, the lower the energy consumption per unit mass, and a higher energy efficiency can be obtained. The calculated SEC function of the plasma spray welding is shown as follows:

$$SEC = \frac{E}{MRM} = \frac{\int P\mathrm{d}t}{v \cdot t} = \frac{\int \left(P_{total} - P_s\right)\mathrm{d}t}{v \cdot t}, \tag{1}$$

where E is the energy consumption used for spray welding in the plasma spray welding process, P_{total} is the total power of the spray welding process, P_s is the standby power of the plasma spray welder, v is the powder feed speed, and t is the spray welding time.

The power curve of the plasma welding machine is shown in Figure 1. The power variation trend under two different parameter settings can be clearly observed from the figure. The figure takes time as the horizontal axis and power (unit: kilowatt) as the vertical axis, visually showing the whole process from the start to the finish of the spray welding. Throughout the entire study range, including all stages shown in the figure, the red curve consistently dominates,

outperforming the black curve both in terms of the growth rate and the height eventually reached. The results show that better performance can be obtained by using parameter 1. The power of the plasma welding machine is different under different process parameters. It can be concluded that there is a certain relationship between the electrical energy consumption in the plasma spray welding process and the process parameters.

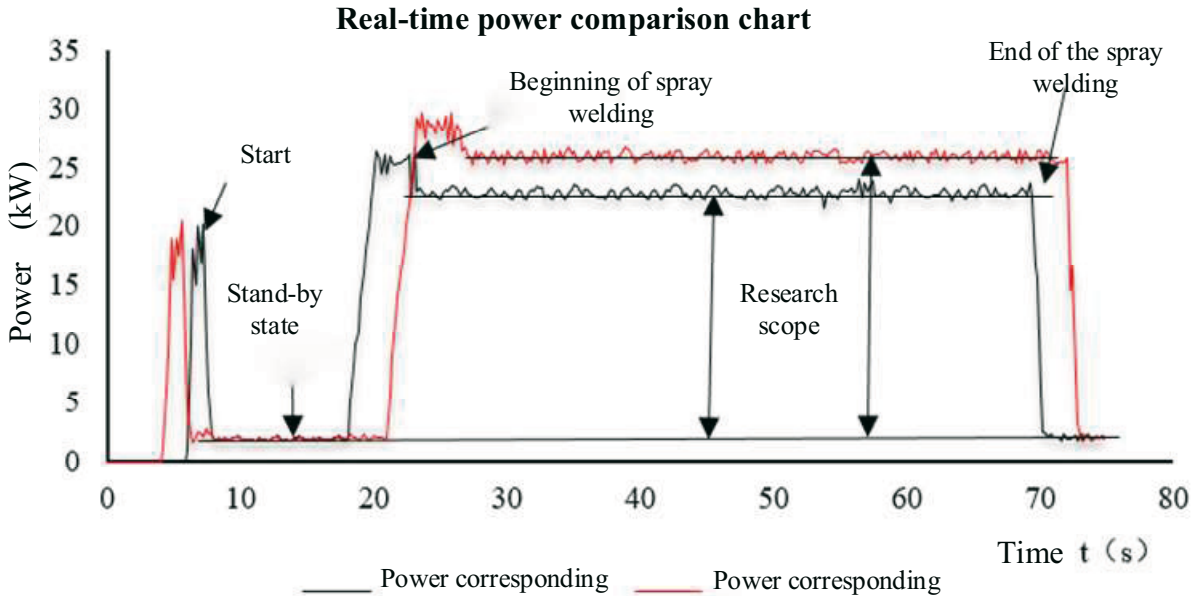

Fig. 1 Power curve of plasma spray welding

2.2 Characterisation of process performance of plasma spray welding used to repair parts

There are many complicated indexes and rules to evaluate the processing property of the parts repaired by plasma spray welding. Based on the former studies of our group, the Vickers hardness and residual stress had a great influence on the processing property of repaired parts. In this paper, the Vickers hardness of the sprayed coating and the residual stress in the heat-affected zone were selected, which greatly influenced the repaired part, to measure the process performance of the parts repaired by applying the plasma spray welding.

1) The Vickers hardness of plasma spray coating

The Vickers hardness is a standard that indicates the hardness of the material. Studies have shown that [23] the Vickers hardness is closely related to wear resistance and fatigue life as well as to process parameters.

2) Residual stress in the heat-affected zone of plasma spray welding

Research shows that [24] plasma spray welding process parameters also closely affect the residual stress of the heat-affected zone in spray welding.

3. Multi-objective optimisation model of processing parameters

Compared with the Box-Benhnken (BBD) test design, the CCD requires multiple continuous tests, and many points will exceed the original level, which is convenient for the fitting of nonlinear equations. The response surface methodology (RSM) can use fewer experimental data to quantitatively analyse the relationships between influencing factors and experimental indices [25]. In this paper, the CCD was applied to test and analyse the relationship between specific energy, the Vickers hardness, residual stress, and process parameters in the plasma spray welding process. Based on the experimental data, the response surface regression equations of the specific energy of plasma spray welding, the Vickers hardness and the residual stress have been established. The specific processes are shown in Figure 2.

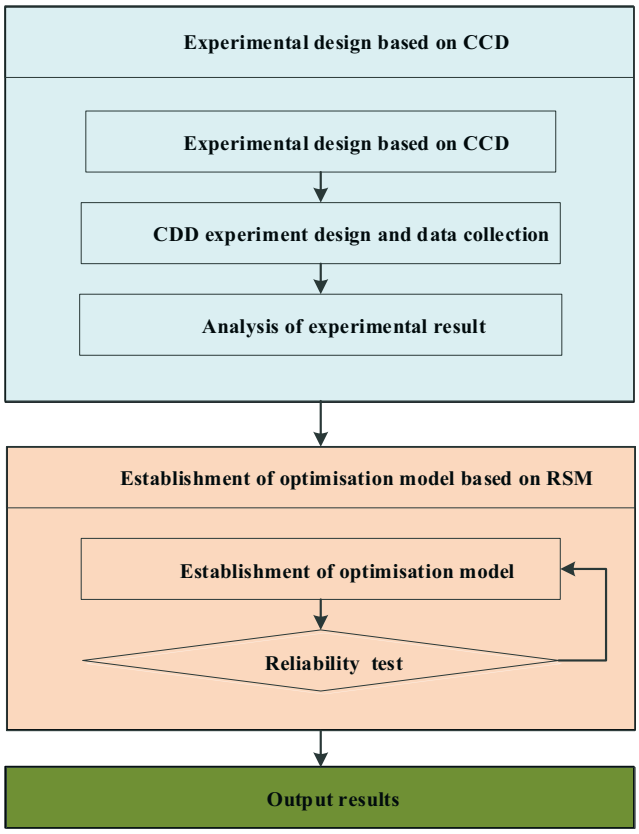

Fig. 2 Modelling process

3.1 CCD-based optimisation experiment design and analysis

The influences of the process parameters on the energy consumption and the process performance of repaired parts in the spray welding process are quite complicated because each parameter is not only related to the other but the parameters also restrict each other. Based on the conclusions of the previous experiments, the rated current, the spray welding speed, and the amount of powder had a great influence on the process performance of the spray-welded repaired parts. Therefore, these three parameters are selected as test parameters.

3.1.1 CCD test design

Table 1 Device information

Equipment		Parameter
Plasma spray welding machine		PTA-400E4-ST general purpose powder plasma spray welding machine, spray welding consumables for Ni60 powder plasma spraying, substrate Q235 
Power acquisition instrument	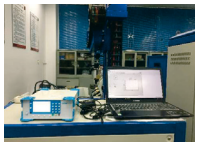	AWS2013 power sensor

Vickers hardness tester		HVS-10Z
Residual stress meter	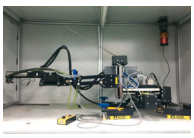	iXRD portable residual stress meter

In the test, a PTA-400E4-ST universal powder plasma spray welding machine developed by the Wuhan Material Protection Institute was used. The spray welding consumable was Ni60 powder, and the test base material was Q235. The power measurement instrument used an AWS2013 power sensor. The power detection field is shown in Table 1. The Vickers hardness measurement instrument used an HVS-10Z automatic turret digital Vickers hardness tester. The residual stress of the repaired part was measured with an iXRD portable residual stress instrument.

In order to ensure the robustness of the CCD model, α is taken as 1.682 [26]. The controllable factor levels and coding are shown in Table 2.

Table 2 Controllable factor levels and codes

Symbol	Level				
	$-\alpha$	− 1	0	+1	$+\alpha$
Spray welding current I / A	106.36	120	140	160	173.64
Spray welding speed V / (mm·min^{-1})	43.18	50	60	70	76.82
Amount of powder v / (g·min^{-1})	7.272	10	14	18	20.728

The value of SEC can be calculated by formula (1) and the total power of spray welding in formula (1) is measured by the power acquisition instrument. When testing the Vickers hardness and the residual stress, the measurement values are quite different because of the different measurement positions. To reduce the experimental errors, according to the central limit theorem, the hardness of the sprayed layer and the residual stress of the workpieces before and after the spraying process (20 mm from the edge of the sprayed layer) were measured each five times, and then they were averaged. The measurement results for combinations of different process parameters of the plasma spray welding are shown in Table 3.

Table 3. Experimental design matrix and experimental results

Standard order	Running order	Factor			SEC SEC / (kJ·g^{-1})	Vickers hardness H / (HV)	Residual stress σ / (MPa)
		X_1 (I)	X_2 (V)	X_3 (v)			
1	18	− 1	− 1	− 1	1.3937	788.5	179.1
2	10	1	− 1	− 1	1.4929	695.9	240.6
3	5	− 1	1	− 1	1.4132	747.6	205.6
4	7	1	1	− 1	1.5114	680.8	269.4
5	4	− 1	− 1	1	1.6593	811.2	114.8
6	6	1	− 1	1	1.9076	730.9	143.1

Standard order	Running order	Factor			SEC SEC / (kJ·g^{-1})	Vickers hardness H / (HV)	Residual stress σ / (MPa)
		X_1 (I)	X_2 (V)	X_3 (v)			
7	8	− 1	1	1	1.6675	740.9	135.8
8	2	1	1	1	1.9272	690.8	193.2
9	17	$-\alpha$	0	0	1.5248	810.8	143.0
10	11	α	0	0	1.8431	684.7	240.3
11	9	0	$-\alpha$	0	1.5734	730.1	168.2
12	13	0	α	0	1.6576	701.5	225.1
13	15	0	0	$-\alpha$	1.2349	723.7	240.2
14	3	0	0	α	1.9087	740.7	112.2
15	14	0	0	0	1.6026	772.5	175.9
16	16	0	0	0	1.6239	768.1	178.6
17	20	0	0	0	1.6107	760.4	179.6
18	19	0	0	0	1.6230	764.4	181.3
19	1	0	0	0	1.6172	765.5	180.9
20	12	0	0	0	1.6217	767.8	177.7

3.1.2 Analysis of test results

The analysis of the main effects showed that the optimal parameter combination was I106.36 V43.81 v7.272 for the smallest specific energy of the spray welding, I106.36 V50 v14 for the lowest Vickers hardness, and I106.36 V43.18 v20.723 for the lowest residual stress. The main effect analysis can directly analyse the rule of influence of each factor on the target and the degree of impact. Overall, it is a kind of experimental method for single objective optimisation, and some adjustments are sometimes required to get the optimal combination from the master effect diagram with respect to the actual processing constraints. Therefore, it is necessary to establish a mathematical model for the target values and conduct a more in-depth study on multi-objective optimisation.

3.2 Establishment of an RSM-based regression model

To optimise the process parameters and build the optimisation objective function, the following second-order response surface model was adopted:

$$Y_u(X) = \beta_0 + \sum_{i=1}^{3} \beta_i x_i + \sum_{i=1}^{3} \beta_{ii} x_i^2 + \sum_{i \le j} \sum \beta_{ij} x_i x_j + \varepsilon \tag{2}$$

where $Y_u(X)(u=1,2,3)$ are the specific energy, the Vickers hardness, and the residual stress, respectively; x_i , x_j $(i, j=1,2,3)$ is each component of the variable parameters; ε is the noise or the error term; $\beta_0, \beta_i, \beta_{ii}, \beta_{ij}$ are the unknown coefficients in which β_i is expressed as the linear effect of x_i; β_{ii} is expressed as the second order effect of x_i; and β_{ij} is expressed as the interaction effect between x_i and x_j.

The formula (3) can be written as the following matrix form:

$$Y_u(X) = D_u \cdot B_u + \varepsilon_u \tag{3}$$

where D_u is the design matrix consisting of the test points, and B_u is the unknown coefficient matrix, which can be obtained by the estimation of the least square method as follows:

$$B_u = \left(D_u^T \cdot B_u\right)^{-1} D_u^T Y_u \tag{4}$$

The response surface model with each optimised index can be obtained by formula (5). A significance test of the response surface model is carried out, the non-significant items in the model are deleted, and the response surface models are obtained.

The response surface model equation of the specific energy is given by

$$\begin{aligned} SEC = {} & 2.15 - 1.8618\times10^{-2} X_1 + 6.0133\times10^{-3} X_2 + 5.8843\times10^{-3} X_3 \\ & + 5.8849\times10^{-5} X_1^2 - 1.0163\times10^{-3} X_3^2 + 4.8531\times10^{-4} X_1 X_3 \end{aligned} \tag{5}$$

where X_1 is the spray welding current, X_2 is the spray welding speed, and X_3 is the amount of powder. The influence of the terms of X_1, X_2, X_3, X_1^2, X_3^2, X_1X_3 on the specific energy is significant, while the rest of the terms do not have significant influence.

The response surface model equation for the Vickers hardness is given by

$$\begin{aligned} H = {} & 251.96 - 0.1936 X_1 + 15.8793 X_2 + 30.8181 X_3 - 1.337\times10^{-2} X_1^2 \\ & - 0.1664 X_2^2 - 0.6777 X_3^2 + 3.5\times10^{-2} X_1 X_2 - 0.17 X_2 X_3 \end{aligned} \tag{6}$$

where X_1 is the spray welding current, X_2 is the spray welding speed, and X_3 is the amount of powder. The influence of the terms of X_1, X_2, X_3, X_1^2, X_2^2, X_3^2, X_1X_3, X_2X_3 on the Vickers hardness is significant, while the rest of the terms do not have significant influence.

The response surface model equation of residual stress is given by

$$\begin{aligned} \sigma = {} & 195.033 - 0.193567 X_1 - 0.922944 X_2 + 8.10126 X_3 \\ & + 1.52\times10^{-3} X_1^2 - 1.17695\times10^{-2} X_2^2 - 8.10703\times10^{-2} \\ & - 1.1122\times10^{-2} X_1 X_3 + 2.1406\times10^{-2} X_2 X_3 \end{aligned} \tag{7}$$

where X_1 is the spray welding current, X_2 is the spray welding speed, and X_3 is the amount of powder. The influence of the terms of X_1, X_2, X_3, X_1^2, X_2^2, X_1X_3, X_2X_3 on the residual stress is significant, while the rest of the terms do not have significant influence.

3.3 Verifying the response surface model

To verify the generalisation capability of the model, nine groups of schemes were selected as test samples. The regression model was used to predict the energy, the Vickers hardness, and the residual stress of the products. At the same time, the schemes were tested to obtain the three indexes of the products. The comparison between the predicted values and the measured values of the test is shown in Figure 3. It can be found that the predicted values can fit well with the experimental data, which represents a good predictive ability of the regression. Although there are still some points, they are all within the allowed error.

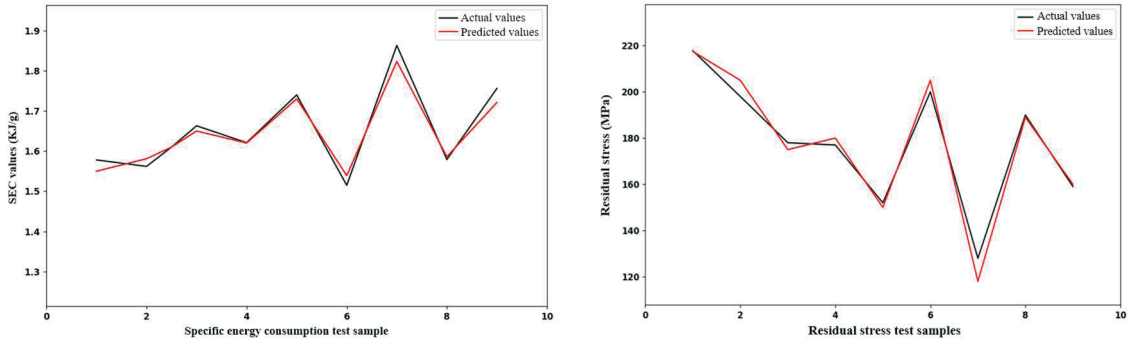

(a) (b)

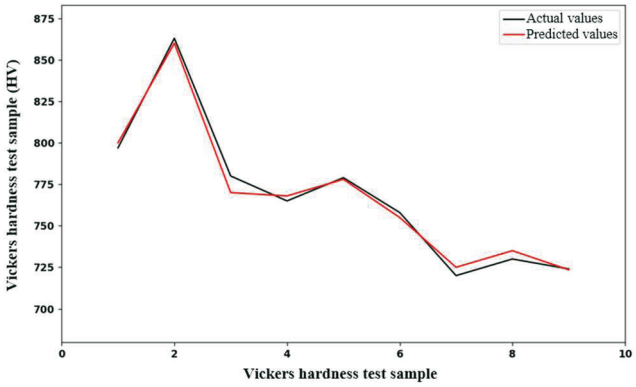

(c)

Fig. 3 Comparison between the predicted values (black line) and the measured values (red line)

At the same time, to further verify the reliability of the model, the multiple correlation coefficient R^2 is used to evaluate [27] the response surface model. The similarities between the calculated values and the actual values are indicated by the R^2 value, which reflects the fitting degree of the response surface model and the test data. The R^2 value ranges from 0 to 1. A good fitting degree of the approximation model can be indicated only if $R^2 > 0.9$. The reliability verification of each model is shown in Table 4.

Table 4 Model reliability verification results

	SEC	h	σ
R^2	0.9883	0.9528	0.960

Table 3 shows that R^2 is greater than 0.9000, indicating that the relationship between the response value and the independent variable is significant. Also, the model can better reflect the data law, and the relationship between the factors can be fully expressed by the model.

3.4 Analysis of interaction between factors of the response surface model

The response surface models of specific energy, the Vickers hardness, the residual stress, and the interaction between various factors can be seen in Figures 4-6. As shown in Figure 4 (a)-(c), the interaction between multiple parameters influence the response value of the specific energy to some extent. From the change of the amplitude of the graph, it is clear that the spray welding current and the powder feeding amount have a more significant influence on the response surface than the spray welding speed. Besides, the specific energy increases with the rise in the spray welding current and the powder feeding amount. The relationship between the specific energy consumption and the spray welding current, the spray welding speed, and the powder feeding amount is monotonically increasing or decreasing.

Figure 5 (a)-(c) shows that the influence of the current and the speed of spray welding on the Vickers hardness of the response surface is more significant. With the increase in the spray welding current, the Vickers hardness decreases. Besides, the Vickers hardness decreases first and then increases with the rise in the spray welding speed. According to Figure 5 (c), when the spray welding current is 140 A, the spraying speed is 55-65 mm/min, and the powder feeding amount is 13-16 g/min, the Vickers hardness increases to the maximum value. Figure 6 (a)-(c) shows that the influence of the spray welding speed on the residual stress response surface is relatively small. The residual stress decreases with the increase in the rotor height or the rise in the powder feeding amount.

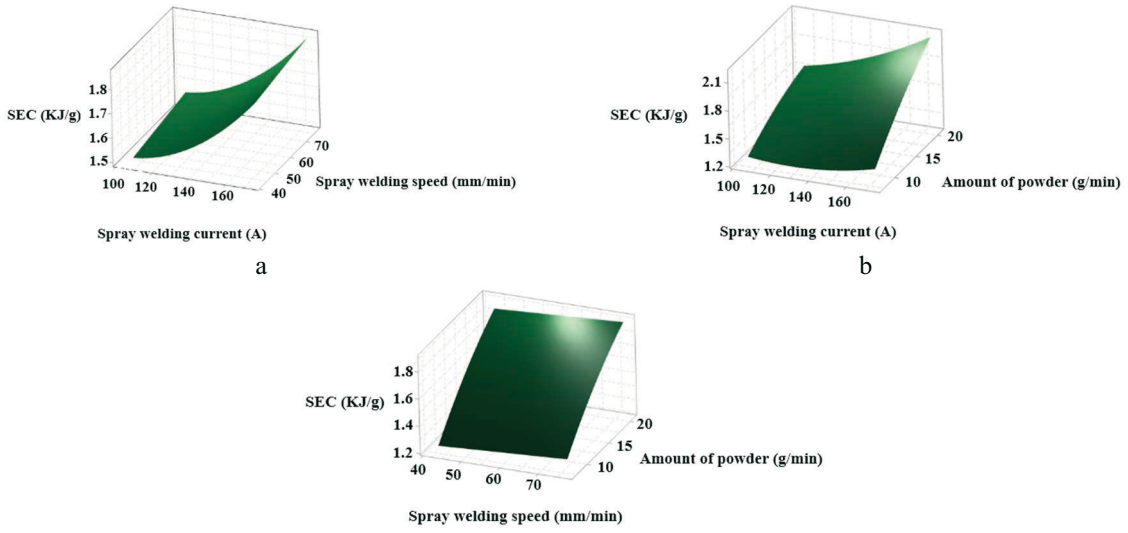

Fig. 4 Effect of interaction between factors on SEC

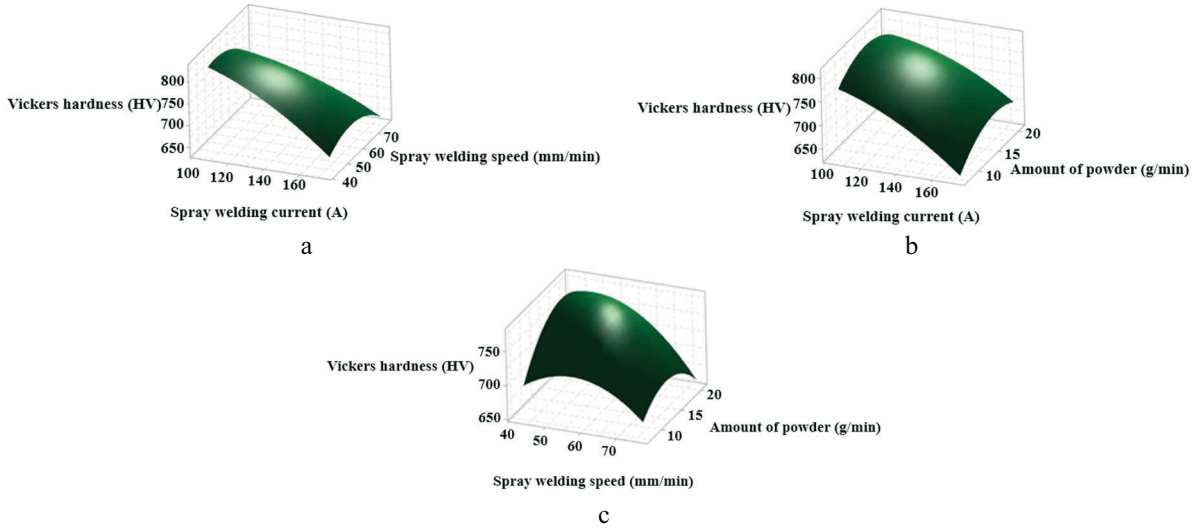

Fig. 5 Effect of interaction between factors on Vicker hardness

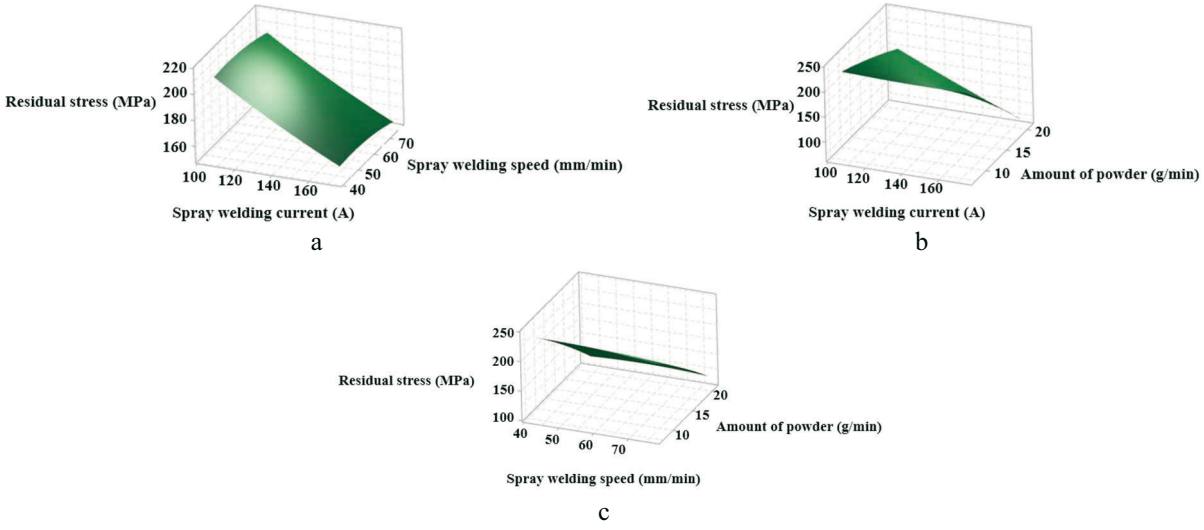

Fig. 6 Effect of interaction between factors on residual stress

4. Model solution based on the NSGA-II algorithm

4.1 Constraint conditions

The parameters of the plasma spray welding process were selected based on whether they satisfied the demands of the processing techniques and conditions of the equipment, after which the constraint conditions were built. The optimised results were more suitable for the actual processing requirements.

The multi-objective optimisation model of the plasma spray welding process parameters is given as follows:

$$\begin{cases} \min SEC(I,V,v) \\ \max H(I,V,v) \\ \min \sigma(I,V,v) \end{cases} s.t \begin{cases} I_{\min} \le I \le I_{\max} \\ V_{\min} \le V \le V_{\max} \\ v_{\min} \le v \le v_{\max} \end{cases} \tag{8}$$

4.2 Model solution

The optimisation of the parameters of the plasma spray welding is much more difficult because of the combination of high dimensions, multiple constraints, and linear and nonlinear intersection. The traditional optimisation algorithm, such as linear programming, can hardly solve that problem. At the same time, the common genetic algorithm itself is prone to premature convergence and falls into the local optimum easily. Therefore, this paper adopted the non-dominated sorting genetic algorithm II (NSGA-II) with a preserving strategy to solve the problem.

The calculation flow chart of the NSGA-II [28] with an elite-preserving strategy and removing repetitive individual procedures is shown in Figure 7.

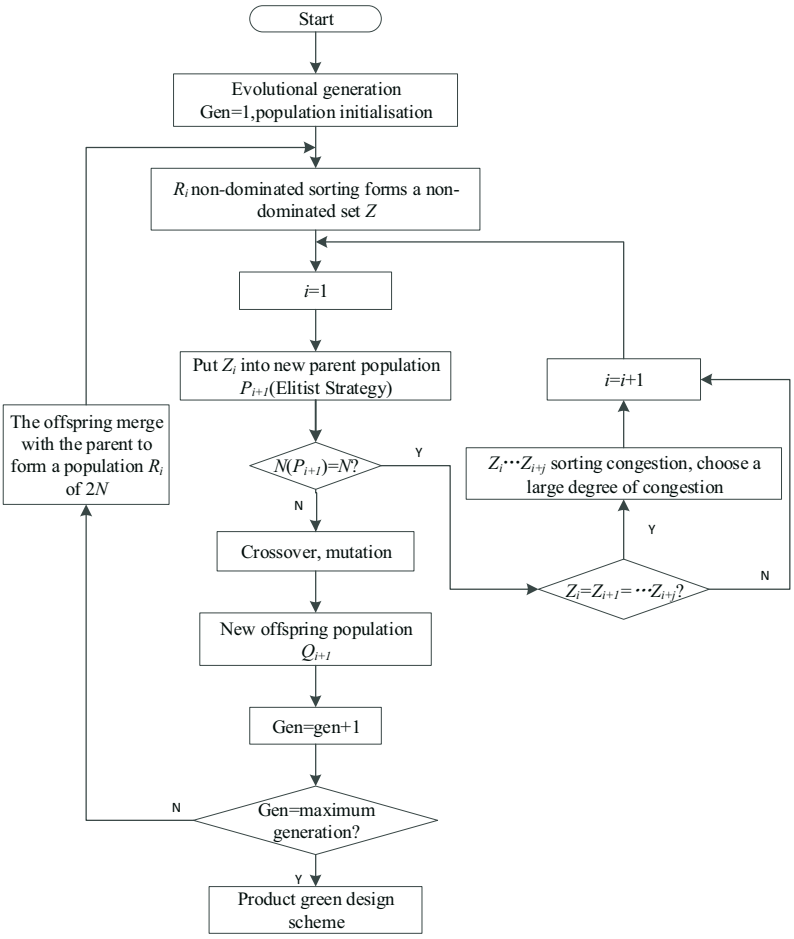

Fig. 7 The calculation process of NSGA-II

Three solutions $x_1\ x_2\ x_3$ of the parent population are selected, and each solution y_k for the intermediate population $y = (y_1, y_2, \ldots, y_n)$ is expressed after the DE cross operation as follows:

$$y_k \begin{cases} x_1 + F\left(x_2 - x_3\right) & if\ p_c < CR \\ x_1 & \text{if } p_c > CR \end{cases} \tag{9}$$

In the formula, F and CR are two control parameters.

The mutation operation of the algorithm adopts a polynomial mutation operator, and each solution in the population after the mutation operation can be described as:

$$\overline{y}_k = \begin{cases} y_k + \sigma_k\left(b_k - a_k\right) & \text{if } p_m < a \\ y_k & \text{if } a < p_m < 1 \end{cases} \tag{10}$$

$$\sigma_k \begin{cases} \left(2 \times rank\right)^{\frac{1}{\beta+1}} - 1 & \text{if } rank < 0.5 \\ 1 - 2 \times \left(2 \times rank\right)^{\frac{1}{\beta+1}} & \text{if } rank > 0.5 \end{cases} \tag{11}$$

where $rank$ is the random number between 0~1, β is the distribution index, p_m is the mutation probability of the algorithm, and a_k and b_k are the lower and the upper limit of the optimisation variable, respectively.

The programming was conducted in Matlab2016a, and four NSGA-II operating parameters were set as follows: the initial population size was 2,000, the number of iterations was 100, the cross probability was 90%, and the mutation probability was 10%. With optimised computation, the optimal value of each objective function was gradually optimised. Variation conditions of each target value during the evolutionary process are given in Figure 8. It can be seen from the figure that the trends of the specific energy consumption, the Vickers hardness, and the residual stress all show good convergence with the increase in iteration times.

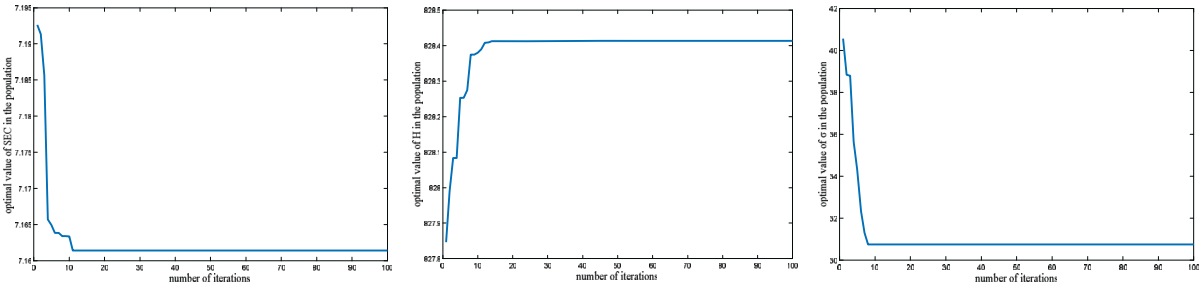

a b c

Fig. 8 Multi-object evolution process: a) optional value of H in the population b) optional value of SEC in the population c) optional value of σ in the population

The obtained Pareto solution is shown in Figure 9a, where the X axis corresponds to the Vickers hardness, the Y axis corresponds to the specific energy consumption, and the Z axis corresponds to the residual stress. It can be seen from the figure that when the Vickers hardness increases, the residual stress increases, and the specific energy consumption decreases, which makes the optimisation goal game-like. The front edge of the three-dimensional Pareto solution is projected to the coordinate plane to obtain a two-dimensional Pareto solution, shown in Figure 9b-d. Based on the analysis of Figure 9, the optimal process

parameters for each single objective are summarised in Table 5. It can be seen from the table that, within a specific range of values, the residual stress is higher when the process combination of the low energy consumption is selected, and the energy consumption is more significant when the process combination of the minor residual stress is selected. The residual stress and the energy consumption are in the middle range when the process combination of the large Vickers hardness is selected. Therefore, there is a group of better process combinations that make the Vickers hardness, the specific energy consumption, and the residual stress have the optimal value.

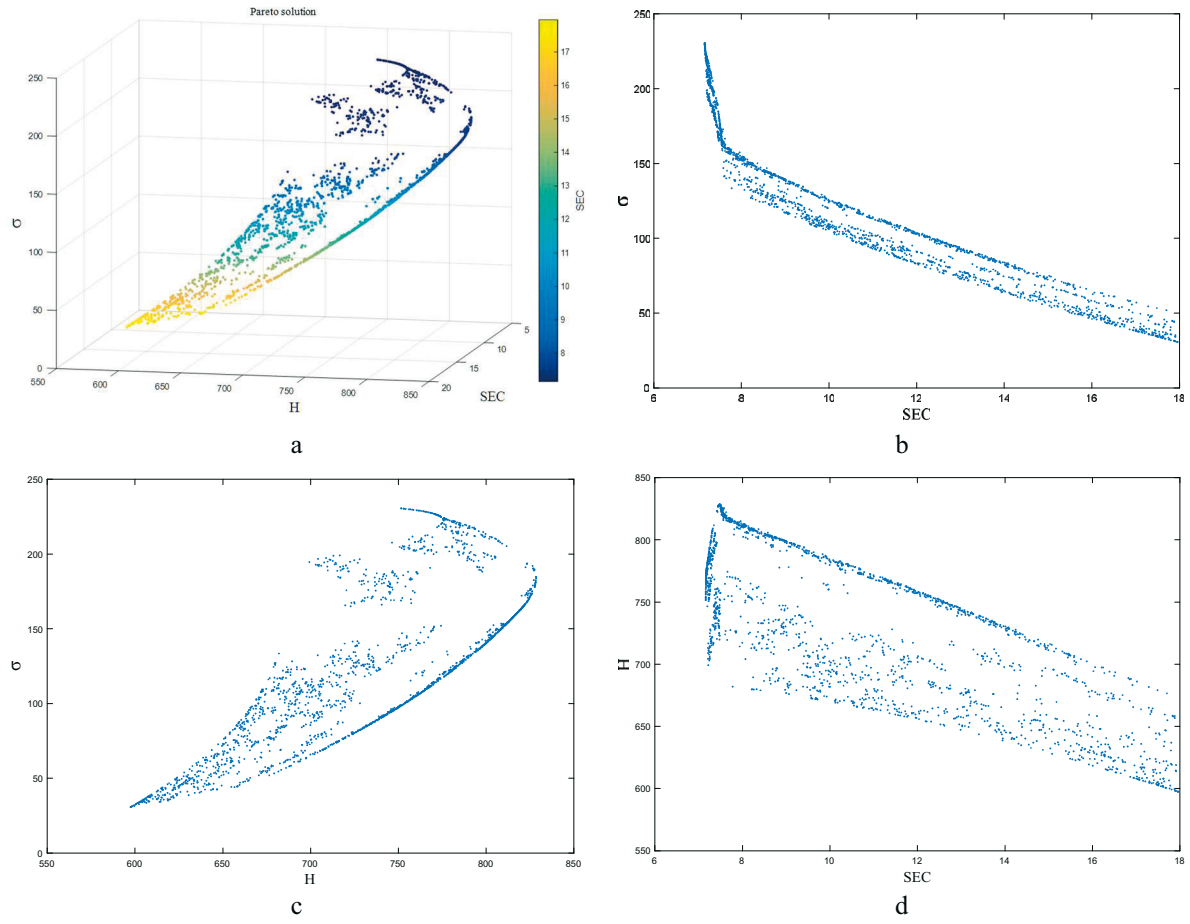

Fig. 9 Pareto value of NSGA-II and its two-dimensional projection:
a) Three-dimensional Pareto solution front, b) Projection on the surface,
c) Projection on the surface, d) Projection on the surface

Table 5 Single objective optimisation results

	Low *SEC* is the optimal objective.	High Vickers hardness is the optimal objective.	Low residual stress is the optimal objective.
SEC / (KJ/g)	7.161	8.226	13.308
H / (HV)	751.617	803.828	669.307
σ / (MPa)	230.486	147.626	74.058
I / A	106.362	111.921	147.477
V / (mm/min)	43.181	54.295	73.505
v / (g/min)	7.272	20.726	20.728

Table 6 Pareto front of optimum combinations

No	*SEC* / (KJ/g)	*H* / (HV)	*σ* / (MPa)	*I* / A	*V* / (mm/min)	*v* / (g/min)
1	10.418	780.617	121.589	128.677	52.358	20.728
2	12.972	743.471	92.909	145.603	56.363	20.728
3	13.301	669.307	74.058	147.477	73.505	20.728
4	9.165	769.918	137.385	119.442	50.129	20.727
5	8.313	802.251	146.265	110.257	54.659	20.725
6	7.459	759.341	174.331	106.360	71.538	14.446
7	10.565	777.791	119.602	129.707	53.474	20.703
8	12.456	745.906	96.364	143.322	58.753	20.728
9	11.124	767.217	111.750	133.552	56.220	20.514
10	15.120	710.131	71.431	158.381	59.424	20.728
11	9.130	795.974	136.736	119.148	52.626	20.727
12	12.023	757.998	103.365	139.572	54.458	20.728
13	8.226	803.828	147.626	111.921	54.295	20.726
14	9.847	700.918	110.621	124.520	73.173	20.701
15	7.264	793.309	212.076	106.361	58.136	9.2643
16	14.018	728.359	82.585	151.970	57.294	20.728
17	8.891	743.840	131.023	117.158	68.632	20.213
18	9.491	700.713	114.622	121.655	73.507	20.726

When single processing properties or the specific energy have the optimal value, the combination properties of the workpieces are usually not optimal, so parts of the optimal solutions were selected through this solution set, as shown in Table 6. To acquire an optimal solution from the Pareto solution set, the decision maker can select the optimal solution from the Pareto solutions acquired through the analytic hierarchy process. The weighted value *w* of each object was acquired through the judgment matrix calculation, which is shown in Table 7. For each solution of the optimal solution set given in Table 8, the corresponding D_i is calculated as

$$D_{\mathrm{i}} = w_S \frac{S_{\max} - S_i}{S_{\max} - S_{\min}} + w_H \frac{H_{\max} - H_i}{H_{\max} - H_{\min}} + w_R \frac{R_{\max} - R_i}{R_{\max} - R_{\min}} \tag{12}$$

where w_{S}, w_{H}, w_{R} are the weights of the target *SEC*, Vickers hardness, and residual stress, respectively. S_{max} and S_{min} are the maximum and minimum of the target *SEC*. H_{max} and H_{min} are the maximum and minimum of the target Vickers hardness. R_{max} and R_{min} are the maximum and minimum of the target residual stress.

The optimal Pareto solution acquired through all obtained D_i is shown in Table 7.

Table 7 Weights of evaluation criteria

Evaluation criterion	Weight
SEC	0.421
Vickers hardness	0.317
residual stress	0.262

Table 8 Results of Pareto optimisation

Energy efficiency	Process performance		Process parameters		
SEC / (KJ/g)	*H* / (HV)	*σ* / (MPa)	*I* / A	*V* / (mm/min)	*v* / (g/min)
12.456	754.906	96.364	143.322	58.753	20.728

5. Results and discussion

Based on the above results, some important conclusions of this study are discussed:

1. The results show that the response surface model we established is effective and reasonable.
2. The acquired Pareto optimality of this problem consists of some points in the three-dimensional space, which are shown in Figure 9 a. All points in this figure represent optimal combinations of the technological parameters, which did not have a mutual effect on each other. Thus, the decision maker can select an optimal machining parameter through an analytic hierarchy process based on expected processing properties and specific energy during the actual processing of workpieces.
3. To make it easier to understand, we used three two-dimensional figures to present the optimisation results. It can be seen from Figure 9 (b-d) that the specific energy increased with a decrease in the residual stress and decreased with an increase in the Vickers hardness, and the residual stress increased with an increase in the Vickers hardness. So, the specific energy and the Vickers hardness could be optimised at the same time.
4. The method put forward in this study can be a useful tool to improve energy efficiency and processing properties of the plasma spray repairing technique.

6. Conclusion

Some conclusions can be drawn from this study.

(1) In this paper, a multi-objective optimisation method was proposed, comprehensively considering specific energy, Vickers hardness, and residual stress. Experimental design was carried out based on CCD to reveal the correlation between various process parameters and optimisation goals through the main effect analysis.

(2) The response surface methodology was used to establish an optimised model using spray welding current, spray welding speed, and powder feed rate as optimised variables. The optimised model was built to achieve the highest energy efficiency and the best process performance of the sprayed welds. The reliability of the model was verified, and the relationship between various factors and goals was fully expressed.

(3) The NSGA-II was used to calculate the optimisation model. Using the three-dimensional Pareto solution, a good balance of the three goals could be found. Through the two-dimensional Pareto solution, we could see that the objective functions were coupled to each other.

(4) According to the method proposed in this paper, within a certain range of process parameters, the optimal combination of process parameters is with the spray welding current being 143.322A, the spray welding speed 58.753 mm/min, and the powder flow rate 20.728 g/min. The energy utilisation rate of the equipment, the Vickers hardness of the repaired layer, and the residual stress of the heat-affected zone can be significantly improved under the preparation of the parameter combination.

(5) For the multi-objective optimisation, it was impossible to get each parameter optimised at the same time. The coordination and compromise among all the parameters must be made to let each parameter be as optimal as possible. From the obtained Pareto solutions, decision makers can select the suitable solutions depending on the actual processing demands.

REFERENCES

[1] Baños R, Manzano-Agugliaro F, Montoya FG, Gil C, Alcayde A, Gómez J. (2011). Optimization methods applied to renewable and sustainable energy: A review. Renewable and Sustainable Energy Reviews 15(4):1753-66. https://doi.org/10.1016/j.rser.2010.12.008

[2] Bunse K, Vodicka M, Schönsleben P, Brülhart M, Ernst FO. (2011). Integrating energy efficiency performance in production management - gap analysis between industrial needs and scientific literature. Journal of Cleaner Production 19(6):667-79. https://doi.org/10.1016/j.jclepro.2010.11.011

[3] Energy Information Administration (EIA). Energy consumption by sector, www.eia.gov/totalenergy/data/monthly/pdf/sec2_3.pdf. 2019, accessed 27 March 2019.

[4] IEA, Market Report Series: Energy Efficiency 2018, https://webstore.iea.org/download/direct/2369?fileName=Market_Report_Series_Energy_Efficiency_2018.pdf. 2019, accessed 27 March 2019.

[5] Wang L, Ran X, Li Y, et al. (2020). Energy consumption model of plasma spraying based on unit process life cycle inventory. Journal of Materials Research and Technology 9(6): 15324-15334. https://doi.org/10.1016/j.jmrt.2020.11.007

[6] Zhang L, He T, Bai Y, et al. (2019). Velocity and temperature of in-flight particles and its significance in determining the microstructure and mechanical properties of TBCs. Acta Metallurgica Sinica (English Letters) 32: 1269-1280. https://doi.org/10.1007/s40195-019-00886-3

[7] Yan W, Zhang H, Jiang Z-g, Hon KKB. (2017). Multi-objective optimization of arc welding parameters: the trade-offs between energy and thermal efficiency. Journal of Cleaner Production 140:1842-9. https://doi.org/10.1016/j.jclepro.2016.03.171

[8] Liu, L., Hao, X. and Song, G. (2006). A new laser-arc hybrid welding technique based on energy conservation, Materials Transactions Vol.47, No.6, pp.1611-1614. https://doi.org/10.2320/matertrans.47.1611

[9] Tian M, Gong X, Yin L, Li H, Ming W, Zhang Z, et al. (2016). Multi-objective optimization of injection molding process parameters in two stages for multiple quality characteristics and energy efficiency using Taguchi method and NSGA-II. The International Journal of Advanced Manufacturing Technology 89(1-4):241-54. https://doi.org/10.1007/s00170-016-9065-7

[10] Sproesser G, Chang YJ, Pittner A, Finkbeiner M, Rethmeier M. (2017). Energy efficiency and environmental impacts of high power gas metal arc welding. The International Journal of Advanced Manufacturing Technology. https://doi.org/10.1007/s00170-017-9996-7

[11] Pastras G, Fysikopoulos A, Chryssolouris G. (2017). A numerical approach to the energy efficiency of laser welding. International Journal of Advanced Manufacturing Technology 92(1-4):1243-53. https://doi.org/10.1007/s00170-017-0187-3

[12] Zhang C, Zhou Z, Tian G, Xie Y, Lin W, Huang Z. (2016). Energy consumption modeling and prediction of the milling process: A multistage perspective. Proceedings of the Institution of Mechanical Engineers, Part B: Journal of Engineering Manufacture. 232(11):1973-85. https://doi.org/10.1177/0954405416682278

[13] Ding H, Guo D, Cheng K, Cui Q. (2013). An investigation on quantitative Analysis of energy consumption and carbon footprint in the grinding process. Proceedings of the Institution of Mechanical Engineers, Part B: Journal of Engineering Manufacture 228(6):950-6. https://doi.org/10.1177/0954405413508280

[14] Yu C, Chen Z, Wang J, Yan S, Yang L. (2012). Effect of welding residual stress on plastic buckling of axially compressed cylindrical shells with patterned welds. Proceedings of the Institution of Mechanical Engineers, Part C: Journal of Mechanical Engineering Science 226(10):2381-92. https://doi.org/10.1177/0954406211433976

[15] Fatima S, Khan M, Jaffery SHI, Ali L, Mujahid M, Butt SI. (2015). Optimization of process parameters for plasma arc welding of austenitic stainless steel (304 L) with low carbon steel (A-36). Proceedings of the Institution of Mechanical Engineers, Part L: Journal of Materials: Design and Applications 230(2):640-53. https://doi.org/10.1177/1464420715584392

[16] Wang X, Wang Y, Song X, et al. (2022). Analysis of thermal shock performance of Y2O3 stabilized ZrO2 (YSZ) coating based on residual stress and micro-morphology. Ceramics International 48(13): 19081-19089. https://doi.org/10.1016/j.ceramint.2022.03.198

[17] Cheng M, Zou X, Pan Y, et al. (2023). Residual stress control using process optimization in directed energy deposition. Materials 16(19): 6610. https://doi.org/10.3390/ma16196610

[18] Ramdan R D, Muhammad Y N, Lumbantoruan S C, et al. (2024). The important factors for structure and mechanical properties in the repair of iron base metal component by thermal spray and welding processes. Eastern-European Journal of Enterprise Technologies 130(12). https://doi.org/10.15587/1729-4061.2024.310239

[19] Han B, Xu W, Zhou K, et al. (2022). Performance analysis of plasma spray Ni60CuMo coatings on a ZL109 via a back propagation neural network model. Surface and Coatings Technology 433: 128121. https://doi.org/10.1016/j.surfcoat.2022.128121

[20] Tao Y, Xiong J, Hui C. (2016). Effect of process parameters on tensile strength in plasma-MIG hybrid welding for 2219 aluminum alloy. The International Journal of Advanced Manufacturing Technology 84(9-12):2413-21. https://doi.org/10.1007/s00170-015-7901-9

[21] Kumar D, Pandey KN. (2015). Optimization of the process parameters in generic thermal barrier coatings using the Taguchi method and grey relational Analysis. Proceedings of the Institution of Mechanical Engineers, Part L: Journal of Materials: Design and Applications 231(7):600-10. https://doi.org/10.1177/1464420715602727

[22] Sarwar, M., Persson, M., Hellbergh, H., et al. (2009). Measurement of specific cutting energy for evaluating the efficiency of bandsawing different workpiece materials. International Journal of Machine Tools & Manufacture 49(12):958-65. https://doi.org/10.1016/j.ijmachtools.2009.06.008

[23] Kumar A, Maheshwari S, Sharma SK. (2015). Optimization of Vickers Hardness and Impact Strength of Silica Based Fluxes for Submerged Arc Welding by Taguchi Method. Materials Today: Proceedings 2(4-5):1092-101. https://doi.org/10.1016/j.matpr.2015.07.014

[24] Lee MJ, Lee BC, Lim JG, Kim MK. (2014). Residual stress analysis of the thermal barrier coating system by considering the plasma spraying process. Journal of Mechanical Science and Technology 28(6):2161-8. https://doi.org/10.1007/s12206-014-0315-z

[25] Abdollahi H, Mahdavinejad R, Ghambari M, Moradi M. (2013). Investigation of green properties of iron/jet-milled grey cast iron compacts by response surface method. Proceedings of the Institution of Mechanical Engineers, Part B: Journal of Engineering Manufacture 228(4):493-503. https://doi.org/10.1177/0954405413502023

[26] Cheng Y, Xu G, Zhu D, Zhu W, Luo L. (2006). Thermal Analysis for indirect liquid cooled multichip module using computational fluid dynamic simulation and response surface methodology. IEEE Transactions on Components and Packaging Technologies 29(1):39-46. https://doi.org/10.1109/TCAPT.2005.848589

[27] Mohammed Iqbal U, Senthil Kumar VS. (2014). Modeling of twist extrusion process parameters of AA6082-T6 alloy by response surface approach. Proceedings of the Institution of Mechanical Engineers, Part B: Journal of Engineering Manufacture 228(11):1458-68. https://doi.org/10.1177/0954405413519606

[28] Deng T, Lin C, Luo J, Chen B. (2018). NSGA-II multi-objectives optimization algorithm for energy management control of hybrid electric vehicle. Proceedings of the Institution of Mechanical Engineers, Part D: Journal of Automobile Engineering 233(4):1023-34. https://doi.org/10.1177/0954407017753446

Submitted: 24.7.2024

Accepted: 26.9.2025

Hejian Liu*
Applied Technology College of Soochow University, Suzhou, 215325, People's Republic of China
Zhen Zhang
School of Mechanical Engineering, Hefei University of Technology, Hefei 230009, People's Republic of China
*Corresponding author:
1_hejian@126.com